Yarn Periodical Errors Determination Using Three Signal Processing Approaches

Vítor H. Carvalho, Michael S. Belsley, Rosa M. Vasconcelos and Filomena O. Soares

Abstract— **This paper presents a study developed for identifying the type and location of yarn periodical errors applying three different signal processing approaches based on FFT – Fast Fourier Transform, FWHT-Fast Walsh-Hadamard Transform and FDFI – Fast Impulse Frequency Determination. Commercial equipment uses exclusively a FFT approach which is not able to clearly detect other yarn periodical types of errors, especially impulse errors. The theoretical description of each signal processing technique is presented, as well as their application to several simulated errors, namely, sinusoidal errors, rectangular errors, pulse errors and impulse errors.**

Index Terms— **Yarn Periodical Errors, Yarn Irregularities, Yarn Hairiness, Walsh – Hadamard, Impulse Frequency Determination**

I. Yarn Periodical Errors

The existence of yarn irregularities occurring with a constant frequency is a dominant source of imperfections in. fabrics. These defects appear as high energy peaks in the frequency analysis [1-3] of yarn characteristics. So, with spectral analysis, it is possible to detect periodic errors in the yarn production process. Hairiness [4-7] (protruding fibers released from the main body of the yarn) (fig. 1) and irregularities [1-3] (fig. 2), (classified as thin places - a decrease in the mass during a short length (4 mm), thick places -an increase in the mass, usually greater than 100% , and lasting more than 4 mm and neps - huge amount of yarn mass in a short length (typically from 1 to 4 mm)), are the major yarn parameters to be analyzed for the occurrence of periodical errors.

Manuscript received 29 September, 2007. This work was supported in part by the Portuguese Foundation (FCT) scholarship (BD/19028/2004).

V. H. Carvalho and F. O. Soares are with the Minho University, Dept. Industrial Electronics, Campus de Azurém, 4800-058 Guimarães, Portugal (phone: +351253510180; fax: +351253180189; e-mail: vcarvalho@ dei.uminho.pt, fsoares@ dei.uminho.pt).

M.S. Belsley is with the Minho University, Dept. of Physics, Campus de Gualtar, 4710-057 Braga, Portugal (e-mail: belsley@ fisica.uminho.pt).

R. M. Vasconcelos, is with the Minho University, Dept. Textile Engineering, Campus de Azurém, 4800-058 Guimarães, Portugal (e-mail: rosa@ det.uminho.pt).

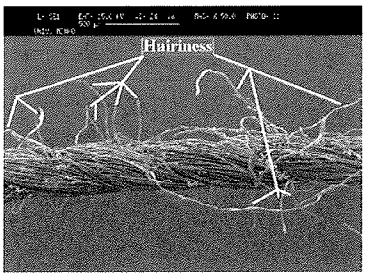

Figure 1 – Yarn Hairiness

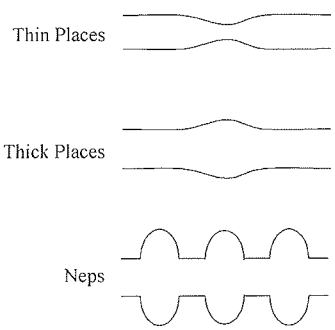

Figure 2 – Yarn irregularities

However, there are two other types of errors [3, 8, 9]:

The first type (fig. 3) typically occurs due to the accumulated dirt at the stretching rollers in the drafting systems, or the displacement of the roller axis, producing a sinusoidal imperfection in the spun yarn diameter.

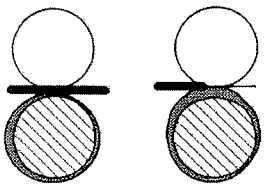

Figure 3 - Accumulated dirt error

The second type (fig. 4) is generally due to imperfections in the surface of the rollers, generating a periodic impulse fault (imperfections in the raw material are seldom periodic).

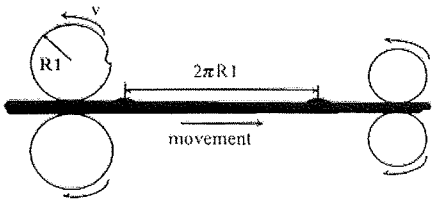

Figure 4 - Imperfection in the surface rollers error

To detect these yarn errors we have used three different signal processing approaches [3] based on FFT (Fast Fourier Transform), FWHT (Fast Walsh Hadamard Transform) and FDFI (Fast Impulse Frequency Determination), instead of a single strategy, based on FFT, as is the case in all present commercial solutions.

II. Signal Processing Approaches Theoretical Considerations

The results obtained are shown in terms of wavelengths (λ (m)), calculated according to equation (1) [1], as they give a more meaningful result to the yarn producer.

$$\lambda = l\frac{f_a}{1000 f_d} \quad (1)$$

Where,

l = step sample length (mm)

f_a = acquisition frequency (Hz)

f_d = detected faults frequencies (Hz)

1) FFT Approach

The first approach is based on the FFT transform [10-12] with a narrow bands definition to aggregate the harmonics, due to the highly concentrated information of the spectrum. This can be considered a periodogram. Equation (2) defines the DFT (Discrete Fourier Transform) one-dimensional determination.

$$F(K) = \frac{1}{N}\sum_{m=0}^{N-1} f(m) e^{-j\frac{2\pi}{N}km} \quad k = 0,1,\ldots,N-1 \quad (2)$$

where,

f –frequency (Hz)

The multiplicative constants can be grouped arbitrary, so the DFT expression can be written as (3).

$$F(K) = \sum_{m=0}^{N-1} f(m) W_N^{Km} \quad k = 0,1,\ldots,N-1 \quad (3)$$

Where,

$$W_N^{Km} = (1/N) e^{-j\frac{2\pi}{N}km} \quad (4)$$

From (3) it is necessary to carry out N complex multiplications and N complex sums, which results effectively in $2N^2$ complex arithmetic operations. FFT algorithm is based on the decomposition of the DFT calculus, in a sequence of longitude N, decreasing each step by half.

Figure 5 shows the FFT algorithm for 8 samples.

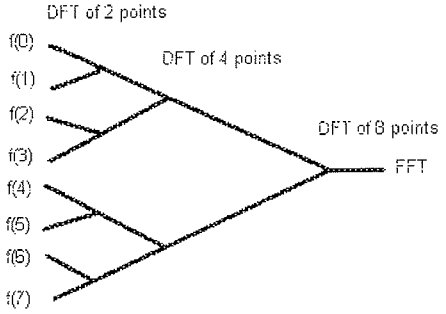

Figure 5- FFT algorithm for 8 samples based on DFT

Considering figure 5, the first step consists of calculating four DFTs of 2 points, the second step, two DFTs of four points and the last step one DFT of 8 points, always based on the previous results.

The final analysis is performed considering the magnitude spectrum (5) using energy bands.

Magnitude spectrum= |F (K)| (5)

The intervals of the energy bands, for each decade, are calculated by (6) [3].

$$\text{int}(j) = \sum_{j=0}^{j=n-1} 10^{i+\frac{j}{n}} \quad (6)$$

Where,

n= number of intervals

i= decade index (-3,…, 4) for [1 mm, 10km]

j= interval index (0,…, n)

Then, all the wavelengths detected, at the corresponding energy band, are summed and then multiplied by its number, obtaining the final value of the energy band (7).

$$e(j) = n\sum_{w=1}^{w=k} \lambda(w) \quad (7)$$

Where,

k= number of detected wavelengths in the band

w= index of detected wavelength

λ (w)= wavelength amplitude at the index w

2) FWHT approach

The Walsh functions create an ordered set of rectangular waves presenting only two possible amplitudes, +1 and -1 [13,14]. They are defined over a limited interval and, as in the case of trigonometric functions, two parameters are necessary for its complete identification. Walsh functions are denoted by WAL (n,t), where t represents the position in the defined interval and n is the order number which is related to the frequency and is equal to the number of sign changes.

Walsh functions are commonly classified using a notation in terms of odd and even symmetries. Two series are presented, the CAL series (odd) and the SAL series (even), which are very similar to the trigonometric series COSIN and SIN, respectively. The CAL (k,t) are symmetric in relation to the mean point of the definition interval, while the SAL functions SAL(k,t) are anti-symmetrical in relation to that point. They are defined by (8) and (9):

$$CAL(k,t) = WAL(2k,t) \quad (8)$$

$$SAL(k,t) = WAL(2k-1,t) \quad (9)$$

where the k parameter is defined as the largest integer less or equal to (n+1)/2.

Three main types of ordering the Walsh functions are known: the sequential, the natural or Hadamard and the dyadic or Paley. In the sequential order, functions are ordered in terms of the sign changes of each wave (fig. 6); in the natural or Hadamard order, the Walsh functions display a nested structure; in the dyadic or Paley order, a Gray Code reordering of the rows is followed. The Hadamard order is the one used in this work, as it is computationally the most efficient. The smallest Hadamard matrix that can be generated is shown in (10). All the other matrices are formed recursively using relation (11), where n is the number of bits in the sample to analyse (2^n samples).

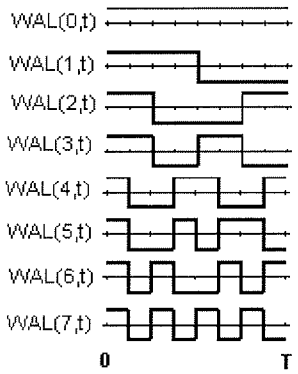

Figure 6 - The first 8 Walsh functions

$$^{1}WH = \begin{bmatrix} 1 & 1 \\ 1 & -1 \end{bmatrix} \quad (10)$$

$$^{n+1}WH = \begin{bmatrix} ^{n}WH & ^{n}WH \\ ^{n}WH & -^{n}WH \end{bmatrix} \quad (11)$$

Figure 7 shows the first 8 Walsh functions ordered by the natural or Hadamard form.

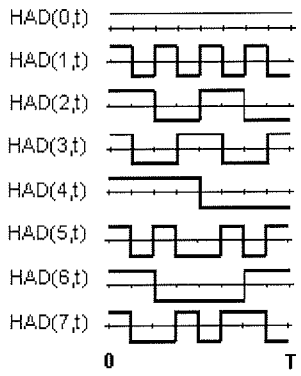

Figure 7 - Hadamard or natural order for 8 samples

The result is an 8x8 matrix, presented in figure 8.

1	1	1	1	1	1	1	1
1	-1	1	-1	1	-1	1	-1
1	1	-1	-1	1	1	-1	-1
1	-1	-1	1	1	-1	-1	1
1	1	1	1	-1	-1	-1	-1
1	-1	1	-1	-1	1	-1	1
1	1	-1	-1	-1	-1	1	1
1	-1	-1	1	-1	1	1	-1

Figure 8 -Hadamard matrix for 8 samples

Finally, the Walsh-Hadamard transform is given by (12).

$$FWHT = \left[x(0) \quad x(1) \quad \ldots \quad x(n-1)\right]^{k} WH \quad (12)$$

Where,

x= array of mass variation (0, 1,…., n-1)
n= 2^k samples

3) DFI Approach

The impulse frequency determination (DFI) is useful in the detection of impulse errors [3, 8, 9]. Furthermore, the sinusoidal, rectangular or pulse errors, are clearly detected by the FFT and FWHT. However, impulse errors are not detected

by the FFT and in the FWHT is not possible to distinguish them from the other referred types. With the DFI they are clearly identified. In the impulse error presented in figure 4, if they exist stretching rollers in addition to those responsible for the error, the error will be extended, causing an impulse error with a longer width. So the DFI Transform was developed [3, 8, 9] to detect this kind of situation, following an approach which consists in the multiplication of an error signal with a coefficient matrix.

The error signal is obtained comparing each sample with a predefined threshold. If the sample amplitude is outside the threshold, the error signal takes the '1' value, otherwise, it takes the value '0'. Afterwards, a matrix is generated, where all the admissible error periods are tested (from n/2 to (n/4)+1, where n represents the number of samples) and phases (initial points). As the n/4 period is multiple of the n/2 period, it is not necessary to test it. In this matrix (R1), the error samples are denoted by '1' or by '0. It has a total number of rows (nl) calculated by equation 13 and a number of columns similar to the number of samples [3, 8, 9].

$$nl = \frac{\frac{N}{2}+\frac{N}{4}+1}{2}\left(\frac{N}{2}-\frac{N}{4}\right) \quad (13)$$

Figure 9 presents an example of a R1 matrix for 8 samples.

$$\begin{vmatrix} 1 & 0 & 0 & 0 & 1 & 0 & 0 & 0 \\ 0 & 1 & 0 & 0 & 0 & 1 & 0 & 0 \\ 0 & 0 & 1 & 0 & 0 & 0 & 1 & 0 \\ 0 & 0 & 0 & 1 & 0 & 0 & 0 & 1 \\ 1 & 0 & 0 & 1 & 0 & 0 & 1 & 0 \\ 0 & 1 & 0 & 0 & 1 & 0 & 0 & 1 \\ 0 & 0 & 1 & 0 & 0 & 1 & 0 & 0 \end{vmatrix}$$

Figure 9 - R1 matrix for eight samples

After generating the R1 matrix, the next step is to create a row matrix which corresponds to the inverse of the number of errors considered in each line of the R1 matrix, multiplied by the number of samples.

Figure 10 presents the R2 matrix derived from matrix R1of figure 9.

$$\begin{vmatrix} 8/2 & 8/2 & 8/2 & 8/2 & 8/3 & 8/3 & 8/2 \end{vmatrix}$$

Figure 10 - R2 matrix for eight samples

Finally, the DFI is obtained by multiplying the error signal, Y(n), with the matrixes R1 and R2, as specified in equation 14.

$$DFI = Y(n)R1 . \times R2 \quad (14)$$

Where, $Y(n)R1 = \sum_{j=1}^{n} c_{ij}$ and C is a coefficient which takes 0 or 1 for a certain row error multiplication (i).

A DFI analysis results in a column matrix, whose row indexes indicate which sample segment contained an error signal. The result can also be represented in terms of a presence function in the interval [0,100] %, from equation 15.

$$a_{\%} = \frac{a(n)}{N} \times 100 \quad (15)$$

Where a is an integer which varies from 0 to N, for a certain tested error row (n)

As an example of the DFI determination, considering the error signal y(n)= [1 0 0 1 0 1 1 1], the belonging percentage results are described in table I.

Table I - Belonging percentage results for each R1 matrix line

a(0)	a(1)	a(2)	a(3)	a(4)	a(5)	a(6)
50%	50%	50%	100%	100%	33.3%	50%

From table I, it is possible to conclude that rows 3 and 4 totally belong to the error (100%), rows 0, 1, 2 and 6 belong in 50% and row 5 belong in 33.3 %. So, the error signal can be decomposed as presented by figure 11.

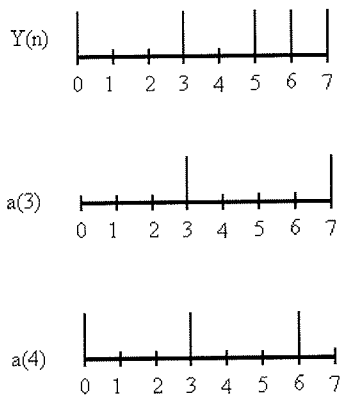

Figure 11 - Error signal decomposition

Although good results were obtained, the previous described algorithm causes computer memory problems if the number of samples is considerable. So, a new version of the algorithm was developed, considering that only the lines which have an index from the error signal are analyzed. This approach is called FDFI, Fast Impulse Frequency Determination.

4) FDFI Approach

The FDFI is based on the determination of a matrix, R3, containing the row indexes that have amplitude 1. This matrix has a number of columns equal to the number of samples and a number of rows equal to the number of periods contained in the R1 matrix.. It is build by placing for each period (matrix row), in a sequential and repetitive form, the indexes of the rows which belong to it [3, 8, 9].

Table II presents an example of the R3 matrix for an 8 samples signal, based on the R1 matrix (Fig. 9)

Table II - R3 matrix for a signal of 8 samples

	i(0)	i(1)	i(2)	i(3)	i(4)	i(5)	i(6)	i(7)
j(0)	0	1	2	3	0	1	2	3
j(1)	4	5	6	4	5	6	4	5

To obtain, the line indexes to analyze, it is only necessary to save in computer memory the first column of matrix R3. Using equation 16 it is possible to obtain the results for the other columns.

$$r_{ij} = MOD(\frac{j}{\frac{N}{2} - i}) + r_{i0} \quad (16)$$

Where, MOD is the remainder of an integer division.

If it was necessary to generate the complete R1 matrix and use the matrix R3 only as pointer indicator for the rows to be analysed, there would be little gain in memory usage. However the matrix R3 can be used to indicate the index of the row to be analysed, as well as to generate the respective row on demand, eliminating the need to save to memory the entire R1 matrix. Furthermore, it is only necessary to generate a number of rows equal to the product of the number of errors detected by the number of generated periods. As an example, for a 16 sample signal in which are detected 8 errors, there are generated 32 rows (eight errors and 4 periods (8, 7, 6, and 5)); all the others have a null value.

The R1 matrix lines, for the indexes considered under matrix R3, are generated under the following algorithm:

$$\begin{cases} Period \leftarrow n/2\text{-}R3\ row\ index\ (from\ 0\ to\ nl/4) \\ r_{ij} \leftarrow MOD(\frac{j}{\frac{N}{2} - i}) + r_{i0} \\ Initial\ Position \leftarrow r_{i,j} - r_{i,0} \\ For\ j \leftarrow 1\ to\ j \le n,\ j \leftarrow j + Period \\ \quad \begin{cases} M[r_{i,j}][j \times Initial\ Position] \leftarrow 1 \\ Initial\ Position \leftarrow 1 \end{cases} \end{cases}$$

In this algorithm, *Initial Position* corresponds to the column index where the first error '1' is encountered, *Period*, corresponds to the number of columns between errors, *Row Index*, corresponds to the row index of matrix R3 to analyse, *nl*, corresponds to the number of rows of matrix R1, *n*, corresponds to the number of samples, being *M* the generated row.

Considering the error signal previously presented, y(n)= [1 0 0 1 0 1 1 1], under FDFI it is only necessary to analyze the rows described in table III.

Table III - R1 matrix line indexes to analyse

Sample index	Rows to analyse
0	0 and 4
3	3 and 4
5	1 and 6
6	2 and 4
7	3 and 5

The final result is a column vector with the number of rows of matrix R1.

III. Experimental Results

In order to test the signal processing approaches we considered a real acquired hairiness variation in reference to the average yarn signal (figure 12 – original signal). Figures 13 and 14, present the results obtained with the FFT and FWHT techniques respectively. Then, four types of simulated errors (periodical sinusoidal error, periodical rectangular error, pulse error and periodical impulse error) were added to the original signal and the spectrograms compared (only a single type of error is considered for each case). A step length acquisition of 1mm was used.

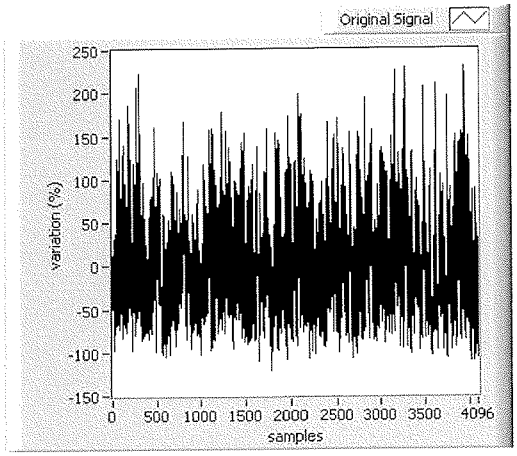

Figure 12 - Original signal

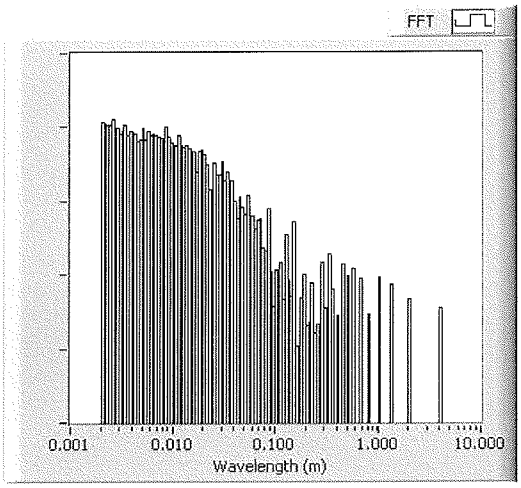

Figure 13 – FFT result for the original signal

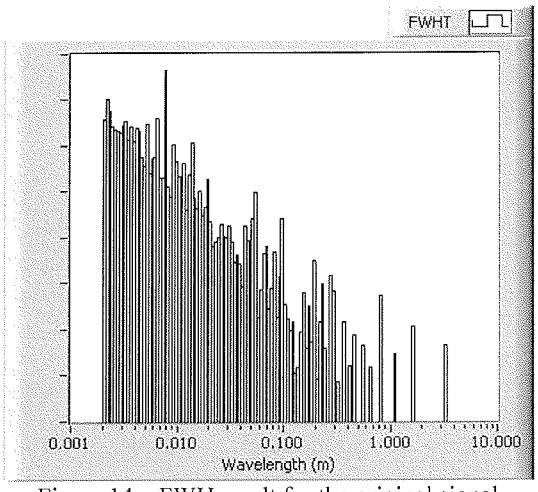

Figure 14 – FWH result for the original signal

Any relevant protruding peaks are not observed in the FFT diagram of figure 13, implying that no clear sinusoidal errors were detected. However, considering the FWHT (fig. 14), a very clear peak appears at 8mm, indicating that a periodic rectangular pattern occurred at that wavelength.

1) Original Signal with a Sinusoidal Error Added Analysis

A periodic sinusoidal error with amplitude of 20 %, over 128 cycles (figures 15 and 16) was added to the initial signal (fig. 12).

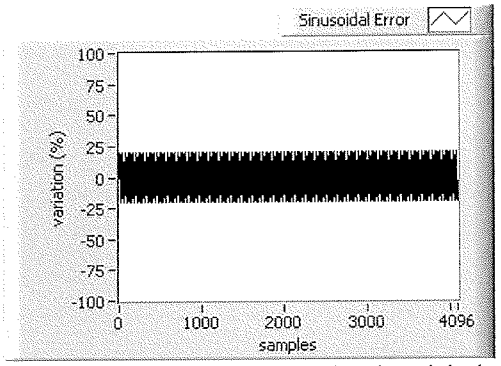

Figure 15 – Full sinusoidal error added to the original signal

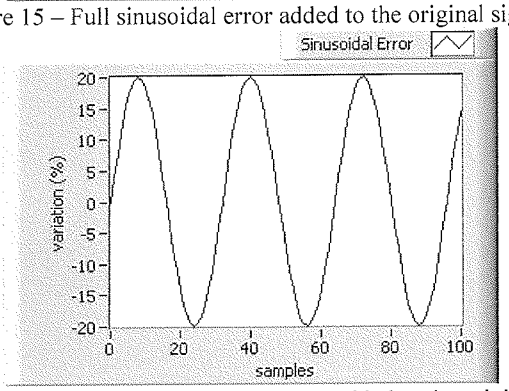

Figure 16 – Zoomed sinusoidal error added to the original signal

The adding result signal is presented by figure 17.

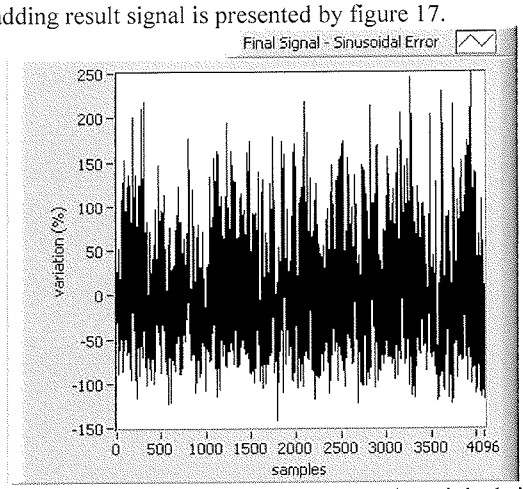

Figure 17 - Addition of sinusoidal error to the original signal

Figures 18 and 19 present the results of FFT and FWHT approach for this situation, respectively.

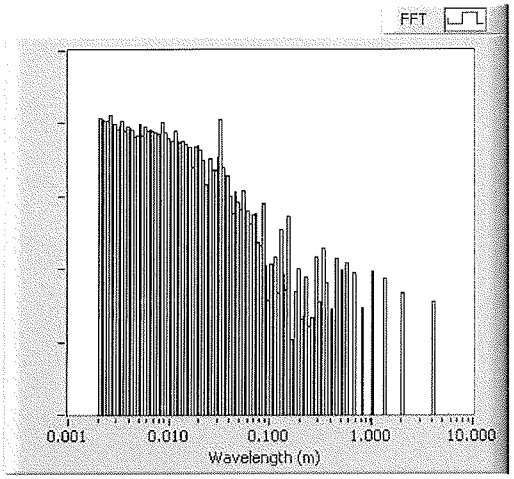

Figure 18 – FFT result for the original signal with the sinusoidal error

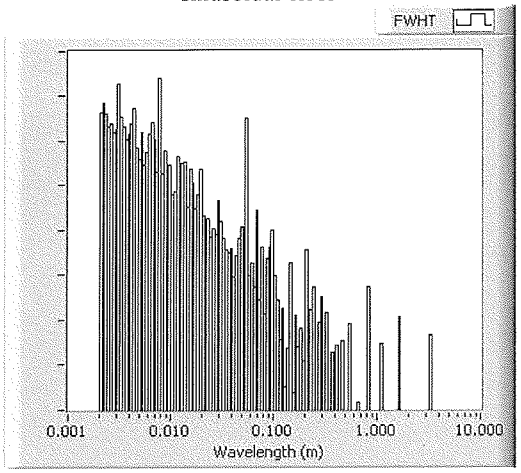

Figure 19 – FWHT result for the original signal with the sinusoidal error

Analysing figure 18 (FFT), it is verified that a relevant protruding peak is now observed around 3 cm, detecting as expected, a clear sinusoidal error at this wavelength. The FWHT spectrogram (fig. 19) also presents, mainly, two new protruding peaks around 3mm and 6 cm. So, as expected, we can verify that a sinusoidal error is also detected by the FWHT, but over several narrow bands. As we know when an error does not match a tested waveform of the applied signal processing technique, it is reflected over several waveforms at different (usually harmonic) wavelengths (decomposition).

2) Original Signal with a Rectangular Error Added Analysis

A positive periodic rectangular error with amplitude of 40 %, over 256 cycles (figure 20 and 21) was added to the initial signal (figure 12).

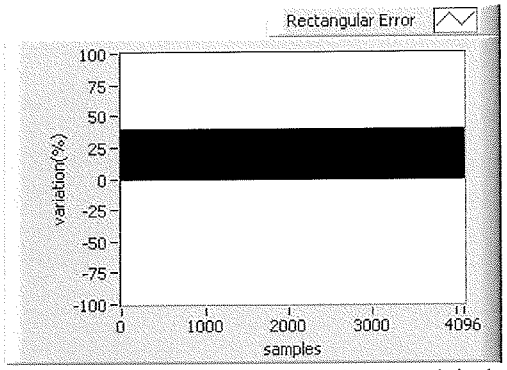

Figure 20 – Full rectangular error added to the original signal

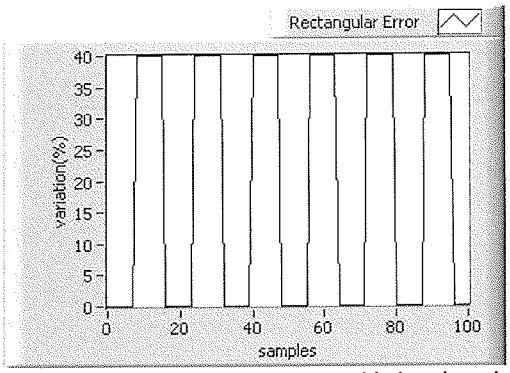

Figure 21 – Zoomed rectangular error added to the original signal

The adding result signal is presented in figure 22.

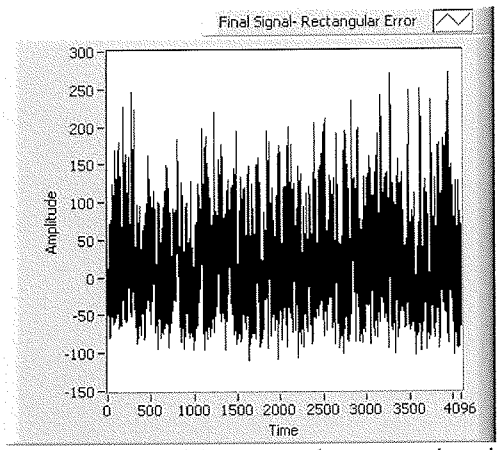

Figure 22 - Addition of the rectangular error to the original signal

Figures 23 and 24, present the results of FFT and FWHT approach for this situation, respectively.

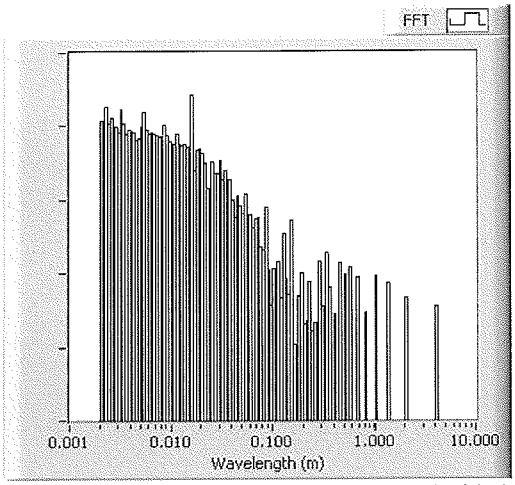

Figure 23 – FFT result for the original signal with the rectangular error

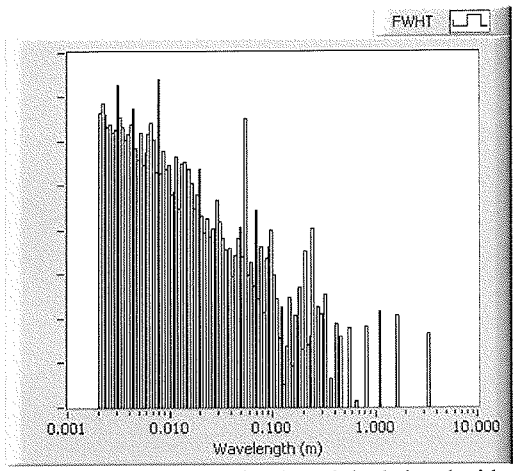

Figure 24 – FWHT result for the original signal with the rectangular error

Figure 23 (FFT), contains a relevant protruding peak at around 2 cm and three others peaks, with minor amplitudes at wavelengths near 2,3 and 5 mm. As expected, we can verify that a rectangular error is also detected by the FFT over several narrow bands in which the main error component clearly protrudes over the spectrogram. The FWHT spectrogram (fig. 24) also presents several new protruding peaks around 3 and 5 mm, 3, 5, 7, 10 and 25 cm. However, the more relevant new protruding peaks are at wavelengths 3mm, 5 and 25 cm. So, we can verify that a periodic rectangular error is also detected over several bands by the FWHT as in the FFT, probably because the added rectangular error does not completely match a tested FWHT waveform. However, in the FWHT the protruded peaks which are also detected in the FFT have higher amplitudes, due to its close similarity to the FWHT waveforms.

3) Original Signal with a Single Pulse Error Added Analysis

A pulse error with amplitude of 100 %, over 256 samples at the beginning (figure 25), was added to the initial signal (figure 12).

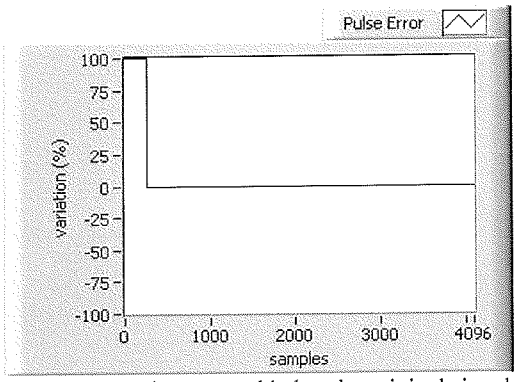

Figure 25 - Pulse error added to the original signal

The adding result signal is presented by figure 26.

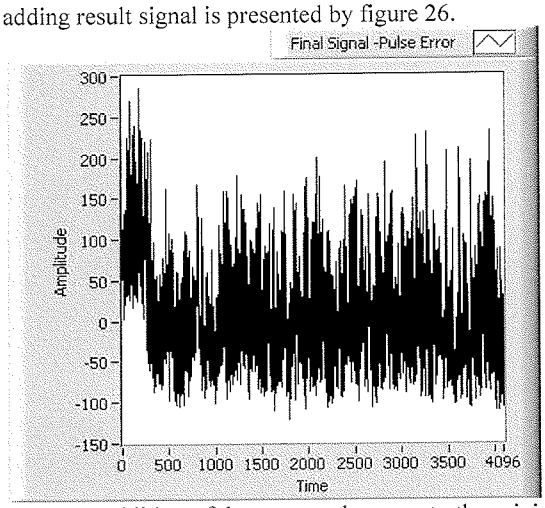

Figure 26 - Addition of the rectangular error to the original signal

Figures 27 and 28, present the results of FFT and FWHT approach for this situation, respectively.

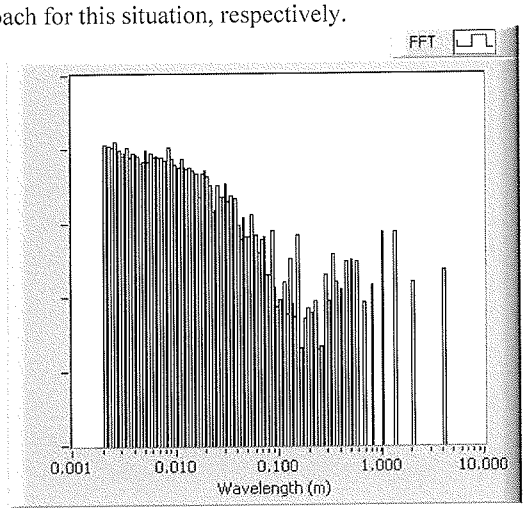

Figure 27 – FFT result for the original signal with the pulse error

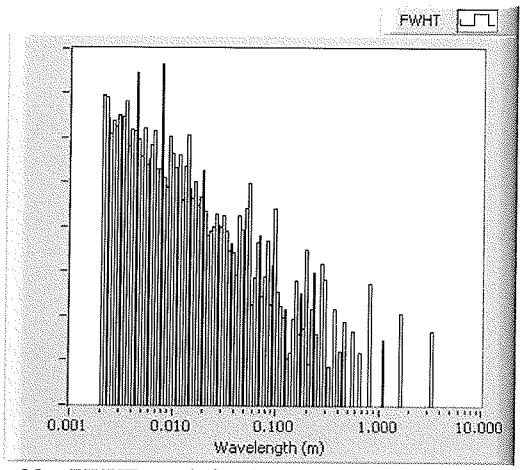

Figure 28 – FWHT result for the original signal with the pulse error

No new protruding peaks are observed in figure 27 (FFT), highlighting that this technique is not at all sensitive to pulse errors. This situation was expected because this is a non periodical error. In FWHT (fig. 28) a new protruding peak is observed around 5mm probably because the simulated error matched a tested waveform of the FWHT technique. It can be concluded that the FWHT could be useful to detect pulse errors.

4) Original Signal with a Periodical Impulse Error Added Analysis

A periodic impulse error with amplitude of 400 % every 384 samples, was added to the initial signal (figure 12), as presented in figure 29.

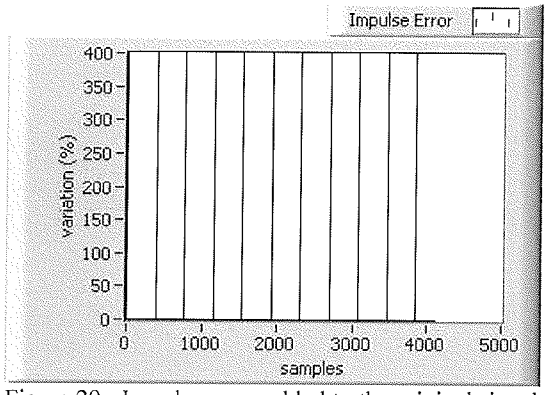

Figure 29 - Impulse error added to the original signal

The resulting signal is presented in figure 30.

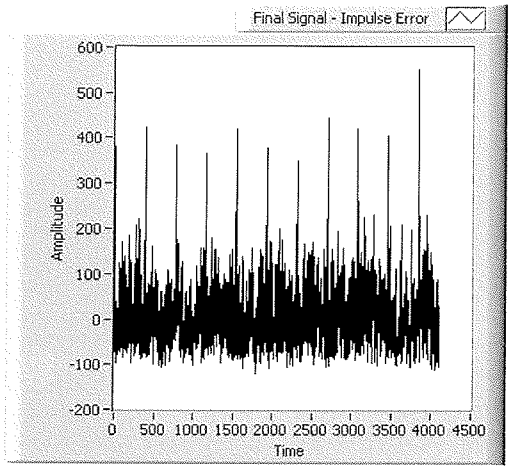

Figure 30 - Addition of the impulse error to the original signal

Figures 31 and 32 present the results of FFT and FWHT approach for this situation, respectively.

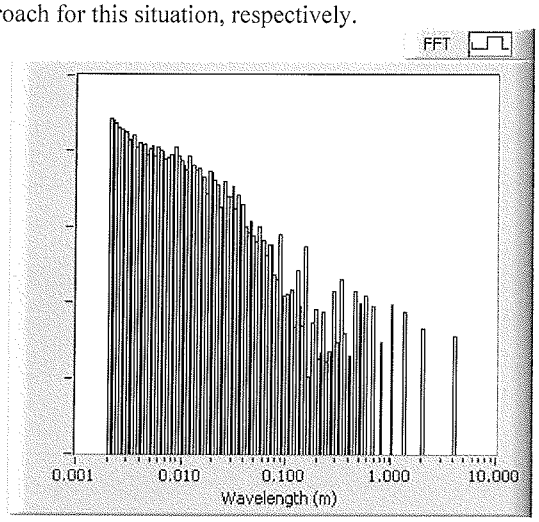

Figure 31 – FFT result for the original signal with the impulse error

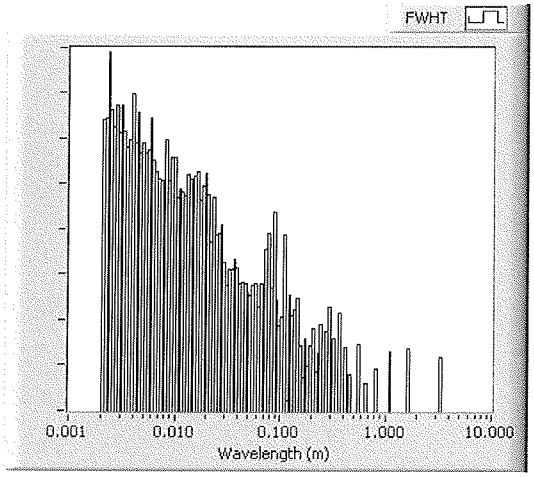

Figure 32 – FWHT result for the original signal with the impulse error

As no new protruding peaks are observed in figure 31 (FFT), this technique seems to be unhelpful to detect impulse errors. In FWHT (fig. 32), several alterations are observed: the main protruding peak of the spectrogram around 8 mm as well as several other ones, were severely reduced while a new protruding peak is observed around 2.5 mm. Finally a reinforcement of the amplitude of the protruding peak around 8 cm occurred. We can thus conclude that although the FWHT detects this type of error, it is impossible to distinguish it, in the spectrogram, from the pulse error. Therefore we turn to the use of the FDFI.

Figures 33 and 34 present the signal processing results based on FDFI, tested for impulse errors with a threshold of 300%.

Figure 33 presents the error signal generated.

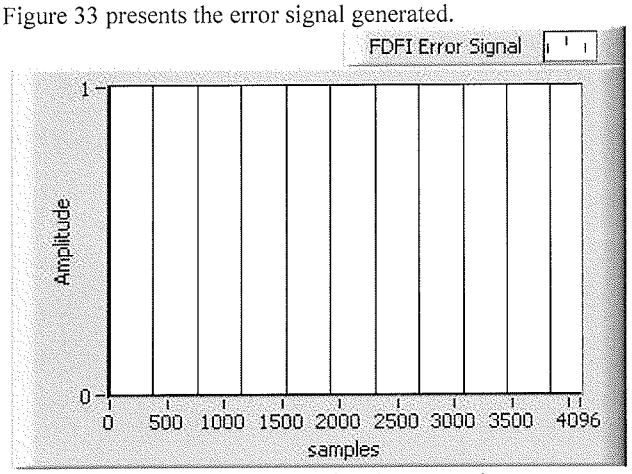

Figure 33 - Error signal generated.

In figure 33 the error signal is distributed over the full range of tested samples in accordance to the threshold defined, because the source signal (fig. 12) as variations of 300% or greater over the identified error signal samples. The considered error samples are 0, 384, 768, 1152, 1536, 1920, 2304, 2688, 3072, 3456 and 3840.

The error signal was subsequently tested with 1573376 periodical impulse errors, resulting from (12) [6, 7], considering a error sample length of 4096.

The signal of row error belongs is presented in figure 34.

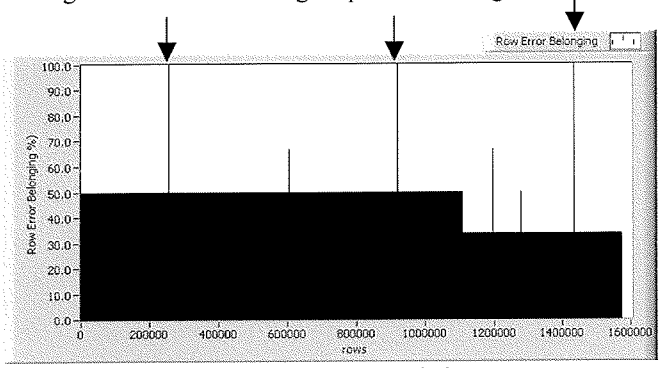

Figure 34 - FDFI row error belongs

Observing figure 34 we can verify that there are identified periodic impulse errors as a result from the 100% row error belongings detection (indicated with arrows in figure 34). These errors are clearly identified in table IV, showing also their initial position, period and number of impulses.

Table IV Description of the detected impulse errors

100 % row error lines	Initial position (sample)	Period (sample)	Number of impulses
254016	0	1920	3
254400	384	1920	2
254784	768	1920	2
255168	1152	1920	2
255552	1536	1920	2
917760	0	1536	3
918144	384	1536	3
918528	768	1536	3
918912	1152	1536	2
1434048	0	1152	4
1434432	384	1152	4
1434816	768	1152	3

As it can be seen in table IV, it is verified that the signal error is decomposed in 12 error lines, with initial positions in indexes 0, 384, 768, 1152 and 1536, containing periods of 1152, 1536 and 1920 samples, resulting in a number of impulses between 2 and 4.

IV. Conclusions and Future Work

Different signal processing techniques based on FFT, FWHT and FDFI were tested in a experimental hairiness spectrogram for error detections. Sinusoidal, rectangular, pulse or periodical impulse errors were added to the original signal.

The previously described analysis allows us to conclude that:

- Periodic sinusoidal errors are clearly distinguished using the FFT approach over a narrow band and in the FWHT over several bands where the main components clearly rise over the spectrum.
- Periodic rectangular error is distinguished in the FFT approach over several bands, where the main error component clearly extends above the spectrum and in the FWHT, also over several bands, if the error does not match the tested waveforms of the technique (if a match is verified a clearly narrow band will protrude).
- Pulse or periodic impulse errors are not detected by the FFT approach but are detected by the FWHT over a narrow band, considering the pulse error and over several bands considering the periodic impulse error. However, it is difficult to distinguish, an impulse

error from a pulse error. For this it is best to use an FDFI analysis.

- Periodic impulse errors are clearly detected by the FDFI approach.

Then, considering the obtained results, we can affirm that a detailed analysis of a detected error requires the use of all three signal processing techniques.

Future work will include the development of new optimized FDFI algorithms in order to reduce the associated computational effort.

ACKNOWLEDGMENT

The authors are grateful to the Portuguese Foundation (FCT) for funding through the scholarship (BD/ 19028/ 2004).

REFERENCES

[1] R. Furter, Evenness Testing in Yarn Production: part I, The Textile Institute and Zellweger Uster AG, Manchester: 1982.
[2] J.S. Neves, A Irregularidade dos Fios Têxteis, sua origem, medição e análise, Oporto: 1968.
[3] V. Carvalho, Parametrização de Fio Têxtil Baseada na Análise de Massa., Msc Thesis, Minho University, Guimarães, Portugal, 2002.
[4] V. Carvalho, P. Cardoso, M. Belsley, R. Vasconcelos and F. Soares, "Determination of Yarn Hairiness Usign Optical Sensors", EUROSENSORS XX, 17-19 September, Gothenburg, Sweden, 2006.
[5] V. Carvalho, P. Cardoso, M. Belsley, R. Vasconcelos and F. Soares, "Development of a Yarn Evenness Measurement and Hairiness Analysis System", IECON06, 7-10 November, Paris, France, 2006.
[6] V. Carvalho, P. Cardoso, M. Belsley, R. Vasconcelos and F. Soares, "Yarn Hairiness Parameterization Using a Coherent Signal Processing Technique", Sensors and Actuators A. Available on-line doi:10.1016/j.sna.2007.02.019.
[7] V. Carvalho, P. Cardoso, M. Belsley, R. Vasconcelos and F. Soares, "A New Statistical Reference Method for Yarn Hairiness Quantification", ISIE 2007, 4-7 June, Vigo, Spain, 2007.
[8] J.L. Monteiro, Sistema distribuído de análise da regularidade de fios têxteis, Minho University, Braga, 1990.
[9] J.L. Monteiro and C. Couto, Pulse frequency calculation and estimation in yarn evenness analysis, IEEE Industrial Electronics Society, Orland, 1995, pp. 985 989.
[10] R.Kuc, Intoduction to Digital Signal Processing, McGraw-Hill, Singapore, 1982.
[11] J.G. Proakis, D. Manolakis, Digital Signal Processing: Algorithms and Applications (3rd Edition), Prentice-Hall, New-York, 1995.
[12] A.V.Oppenheim, A.S. Willsky, Signals and Systems (2nd Edition), Prentice-Hall, New-York, 1996.
[13] B. Golubov, A.Efimov, V. Skvortsov, Walsh Series and Transforms: Theory and Applications, Springer, New York, 2006.
[14] S. Tzafestass, Walsh Functions in Signal and Systems Analysis and Design, Springer, New York, 1985.

Vitor H. Carvalho received his degree in industrial electronics engineering in the option of telecommunications and industrial informatics, in 2002 and MSc in industrial electronics, in the option of automation and robotics in 2004, both from Minho University, Portugal. At present he his preparing is PhD in industrial electronics which covers the subject presented here while working as lecturer, since 2005, at IPCA and UCP. His main fields of interest are data acquisition and signal processing.

Michael S. Belsley obtained his PhD degree in physics from the University of Colorado at Boulder in 1986. He then worked at the California State University in Long Beach, Oxford University and the University of Oregon before coming to Minho University in Braga Portugal where he has lectured as an associate professor of physics since 1992. His main fields of interest are laser spectroscopy and nonlinear optics.

Rosa M. Vasconcelos received her degree in textile engineering, in 1984 at Minho University, Portugal. In 1993 she obtained her PhD in Engineering-Textile Technology and Chemistry on the speciality of Textile Technology, in Minho University. Since 2005 she is working as associate professor, in the Textile Engineering Department of Minho University. Her fields of interest are textile processes and industrial automation.

Filomena O. Soares received her degree in chemical engineering, in 1986 at Porto University, Portugal. In 1997 she obtained her PhD in Chemical Engineering in Porto University. Since 2007 she is working as associate professor, in the Industrial Electronics Department of Minho University. Her fields of interest are process modelling and control and process automation.